Korean Journal of Polar Research
Vol.2, No.1(Spec. Issue), p.107~134, June 1991

Petrology and Geochemistry of the Volcano-plutonic Rocks in the Barton and the Weaver Peninsula, King George Island, Antarctica

Myung-Shik Jin[1], Min-Sung Lee[2], Pil-Chong Kang[1], and Yong-Joo Jwa[3]

1) *Korea Institute of Energy and Resources*
P.O.Box 5, Daedeok Science Town, Dae jeon, 305-343, Korea
2) *Department of Earth Science, College of Teachers*
Seoul National University
Shinlim-dong, Gwanag-gu, Seoul, 151-742, Korea
3) *Polar Research Center*
Korea Ocean Research and Development Institute
Ansan P.O.Box 29, Seoul, 425-600, Korea

Abstract : Volcano-plutonic rocks distributed in the Barton and Weaver Peninsulas of King George Island, Antarctica range in composition from basaltic through andesitic and dacitic to rhyodacitic and/or quartz-dioritic rocks and have radiometric age of Early Tertiary times.

Major and trace element geochemistry for the rocks support that they have been fractionated from a calc-alkaline magma, generated by the partial melting of old oceanic crust and/or mantle. The REE pattern for the rocks in a strong evidence for the same genesis for the volcano-plutonic rocks.

Key words : calc-alkaline, I-type, Sr initial ratio, REE pattern, King George Island, Barton peninsula, Weaver peninsula, Antarctica

Introduction

On the geology of the Barton Peninsula and its neighboring areas, many important papers (Hawkes, 1961; Adie, 1962; Barton, 1965; Grikurov et al., 1970; Thomson, 1972; Rex, 1976; Davies, 1972; among others) have been published since the issue of the first literature (Ferguson, 1921). Upon the opportunity of the establishment of the King Sejong Station in the Barton Peninsula in 1987, Korean scientists have accelerated Antarctic researches. Consequently, a few geological studies (Hong, 1989; Kang and Jin, 1989; Park, 1989) have been carried out.

This article is the report of a 10 day's field survey and laboratory works in the fields of geology, petrology and geochemistry of the Barton and Weaver Peninsulas.

The survey trip was made in 1989 as a part of the 2nd Korea Antarctic Research Programme of the Korea Ocean Research and Development Institute (KORDI).

This paper aims first to classify and characterize the petrological and geochemical natures of the volcano-plutonic rocks distributed in the Barton and Weaver Peninsulas, and second to interpret the geological and tectonic setting of the study area.

Geomorphology

The Barton and Weaver Peninsulas face each other across the Marian Cove, and approximately half of the Peninsulas are covered by glacier and moraines as described by

the previous workers (Barton, 1965; Davies, 1982; Kang and Jin, 1989). U-shaped valleys, cirques, glacial lakes, inselbergs, and polygon structures on the ground, which are the typical geomorphological features of the Antarctica, are ubiquitous in the study area. Glacial tracks, running in two different directions, are left for the detailed examination of orientations of moraines exposed in the back of the King Sejong Station. The moraines, consisting of various sizes of sediments from clay to boulder, contain volcanic clasts which might be derived within the peninsulas.

In addition, clasts of mostly pebble size are distributed along the elevated old beaches, which are placed at the levels of 3−4 m, 20 m, 100 m, 150 m and 250 m above the present sea level.

General Geology

The oldest rocks in the Barton Peninsula are purple volcanogenic breccia and pebble bearing purple and greenish siltstone, which are overlain by the agglomerate consisting mostly of basaltic to andesitic breccias and smaller clasts (Fig. 1). Intermediate to acidic volcanic rocks, mainly ash-flow tuff, cover unconformably the aforesaid rocks. These sedimentations of volcanic and volcaniclastic rocks were intruded by hypabyssal basaltic porphyry and quartz-diorite. Those geological activities were resulted from volcano-plutonisms during the Early Tertiary times (Grikurov et al., 1970; Davies, 1982; Kang and Jin, 1989) (Fig. 1).

The geology of the Weaver Peninsula is much similar to that of the Barton Peninsula, except the fact that volcanic rocks in the Weaver are mostly pyroclastic and more basic than those of the Barton. The volcanic rocks of the Weaver Peninsula are commonly agglomerates in the southwestern coastal area and mostly ash-flow tuffs in the upper inside of the Peninsula. Exceptionally, hypabyssal basaltic porphyry crops out in the southeastern coastal area (Fig. 1). Clasts of the agglomerates are chiefly basaltic to andesitic boulders, and the ash-flow tuffs are also mostly basaltic to andesitic in composition. Propylitic and argillic alteration are widely recognized in the northwestern and southern parts of the Barton Peninsula suggesting that metallic and non-metallic deposits could be formed.

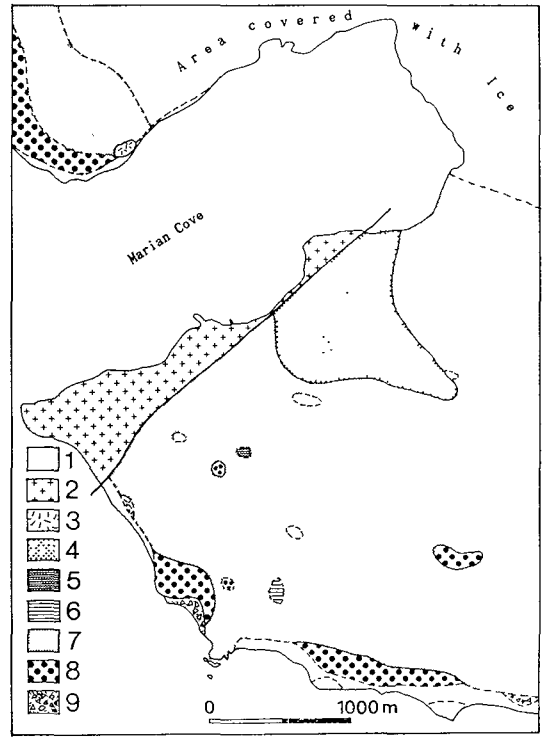

Fig. 1. Geologic map of the Barton and Weaver Peninsulas around the King Sejong Station of the Republic of Korea.
Legend : 1. Beach gravel ; 2. Quartz−diorite ; 3. Basaltic andesite porphyry ; 4. Crystal tuff ; 5. Bedded tuff ; 6. Sedimentary Rock ; 7. Lithic and Ash−flow tuff;8. Agglomerate ; 9. Breccia with subordinate siltstone

Petrography

1. Breccia and pebble bearing siltstone

The breccia bed, 3−4 m thick and containing boulders and breccias of volcanic rocks is distributed in the southwestern and southern coast of the Barton Peninsula. These layers of pebble bearing purple siltstone are interlayered in the breccia. The breccia bed strikes N75° E and 20° SE (Fig. 2). These rocks are overlain by agglomerates in the southwestern coast and by ash-flow, lithic tuffs along the southern coast.

Fig. 2. A photograph of the breccia bed with subordiante siltstone distributed in the southwestern coast of the Barton Peninsula.

In addition, pebble bearing fine purple sandstone or siltstone crops out along the southern coast, about 700−800 m away from the Halla Hill. The sandstone strikes N10° W and dips 25° SW. The sandstone is rather well sorted and contains purple or grey volcanic pebbles ranging 1−2 cm in diameter (Fig. 3).

2. Agglomerates

The agglomerate rests on the breccia and is overlain by lapilli tuff or lithic tuff in the western and southern parts of the Barton Peninsula (Fig. 1). The clasts of the agglomerate are mostly dark grey and purple, basaltic to acidic

Fig. 3. A photograph of the pebble bearing purple siltstone distributed in the southern coast of the Barton Peninsula.

tuffaceous rock fragments ranging from several cm to a few tens of cm in diameter. Although the sorting is poor, the stratification of the agglomerate is easily recognized (Fig. 4). Strikes and dips of the agglomerate beds highly differ from place to place, caused probably by uneven topography of volcanic areas.

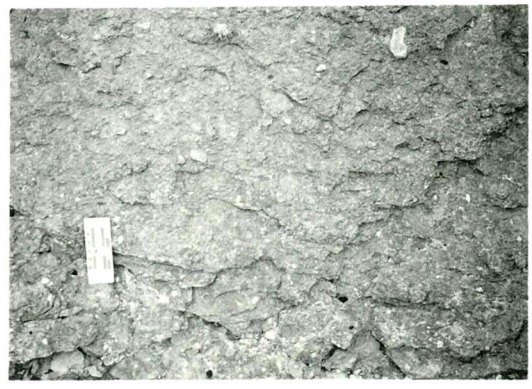

Fig. 4. A photograph of the agglomerate distributed in the southwestern coast of the Barton Peninsula.

In contrast, the agglomerates of the Weaver Peninsula contain the clasts of basaltic to intermediate volcanic rocks, which are larger in average diameter. The agglomerate beds strike

N50° E and dip 40° SE.

3. Tuffs

Lithic tuff, crystal tuff and suboridnately bedded tuff are most widely distributed in the Barton and Weaver Peninsulas (Fig. 1). The lithic tuff shows evidences of ash-flow origin, such as eutaxitic flow texture under the microscope (Fig. 5). The lithic tuff is characterized by the

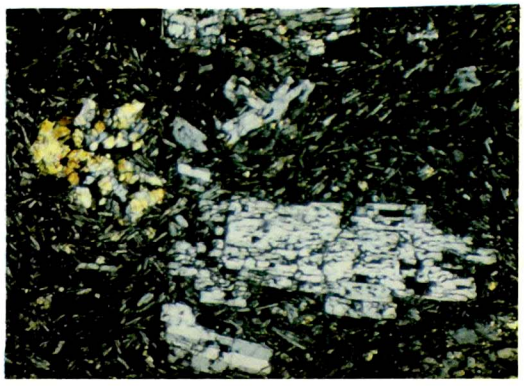

Fig. 5. A photomicrograph shows an eutaxitic flow texture of the ash-flow tuff distributed in the Barton Peninsula.

phenocrysts of euhedral and subhedral plagioclase, olivine, pyroxene and hornblende crystals, which are set in the groundmass consisting of plagioclase laths and opaque minerals (Fig. 6).

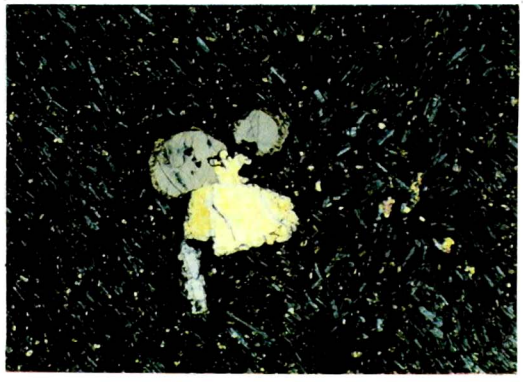

Fig. 6. A photomicrograph shows pyroxenes and olivine pheocrysts with flow textured laths of plagioclase(in crossed nicols).

The plagioclase phencrysts commonly show carlsbad twinning of which plane is relatively wide, and zonal texture is not common. Some of the plagioclase oikocrysts contain tiny anhedral chadacrysts of pyroxene (Fig. 7). The hornblende phenocrysts are mostly carlsbad twinned subhedral crystals with pale to dark green plechroism. The plagioclase and hornblende crystals are partly altered into seri-

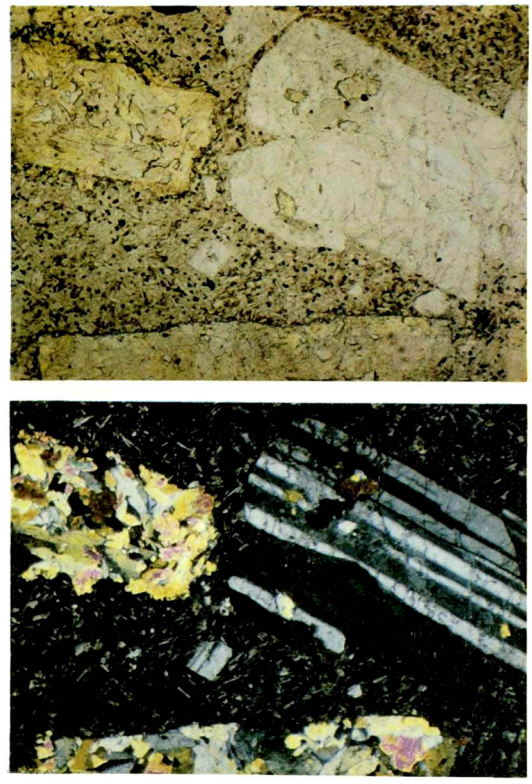

Fig. 7. A photomicrograph shows a plagioclase phenocryst containing a lot of tiny secondary epidotes in the groundmass of fine laths(A. in open nicols ; B. in crossed nicols)

cite, epidote, calcite, quartz and opaque minerals.

The relationship between the ash-flow tuff and lithic tuff is not clear, but transitional to each other. The crystal tuff distributed around the Seolag-bong, has often been classified as

quartz-diorite or granodiorite by previous workers. The distinction between the tuff and quartz-diorite is often uncertain because they share similar mineral and chemical composition and petrographical features (Barton, 1965; Grikurov, 1970; Davies, 1972). However, on detailed examination of the weathering pattern on the surface and textures in this section, pyroclastic origin of the crystal tuff around the Seolag-bong is evidenced not only by having a typical weathering pattern of tuffaceous rocks (Fig. 8), but also by showing a typical pyroclastic texture (Fig. 9). The crystal tuff comprises plagioclase, alkali-feldspar, hornblende, biotite, quartz, opaque mineral and secondary minerals such as sericte and chlorite as in the quartz-diorite.

Fig. 8. A typical weathering pattern of crystal tuff discriminating it from granite in the northwestern part of the Barton Peninsula.

The field relationship between the crystal tuff and the quartzdiorite is not clear, but they are now contacted by fault covered with the talus of the crystal tuff debris.

The bedded tuff distributed around the Kwanak-bong, central part of the peninsula (Fig. 10) occurs as a small mound in the southern part of the peninsula.

4. Volcanogenic fine sandstone

Above the ash-flow tuff, 30–40 m thick

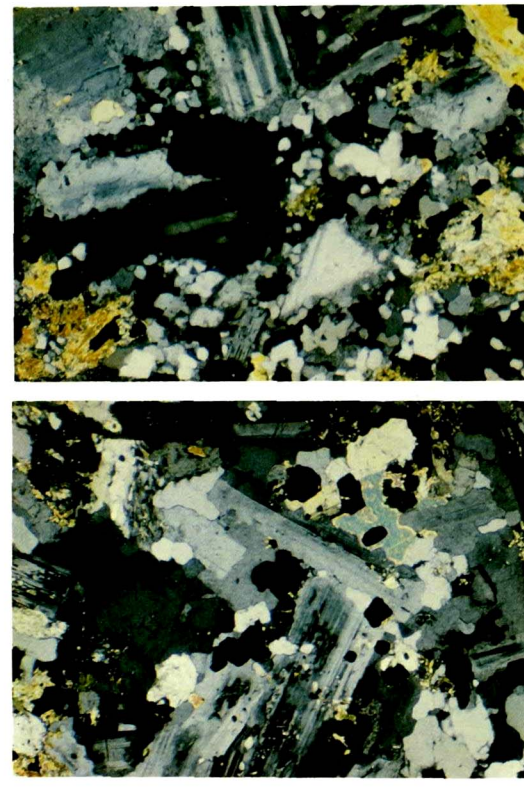

Fig. 9. A photomicrograph shows a typical texture of crystal tuff containing plagioclase, biotite, hornblende, fine vitric crystals and opaque minerals as in sedimentary rocks.

Fig. 10. Bedded tuff distributed around the Kwanag–bong shows relatively good bedding plane.

volcanogenic fine sandstone sequence with subordinate siltstone layers, is exposed in an area 50−60 m wide and about 100 m long. In addition to the area, volcanogenic fine sandstone is distributed in a small area, about 500 m northeast of the Candle Stone, in the southern part of the Barton Peninsula. The sandstone, striking N20°E and dipping 10°SE (Fig. 1), is characterized by yellowish to reddish brown color caused by oxidation of disseminated pyrites on the surface (Fig. 11). In places the sandstone sequences rock is an alternation of 15−20 cm thick light grey fine sandstone and 5 cm thick dark grey to black siltstones.

Fig. 11. An outcrop of the volcanogenic fine sandstone shows pronounced bedding and no variation in grain size, in the southern part of the Barton Peninsula.

Under the microscope, the sandstone is composed of well sorted silt to fine sand sized grains and subhedral opaque minerals. As the sand sized grains appear to be altered to secondary calcites or clay minerals, so grain boundaries among them are commonly not clear as effected by diagenesis (Fig. 12).

5. Basaltic andesite porphyry

The basaltic andesite porphyry crops out as small stocks (20 m x 20 m), in the southwestern coast of the Barton Peninsula and southeastern coast of the Weaver Peninsula.

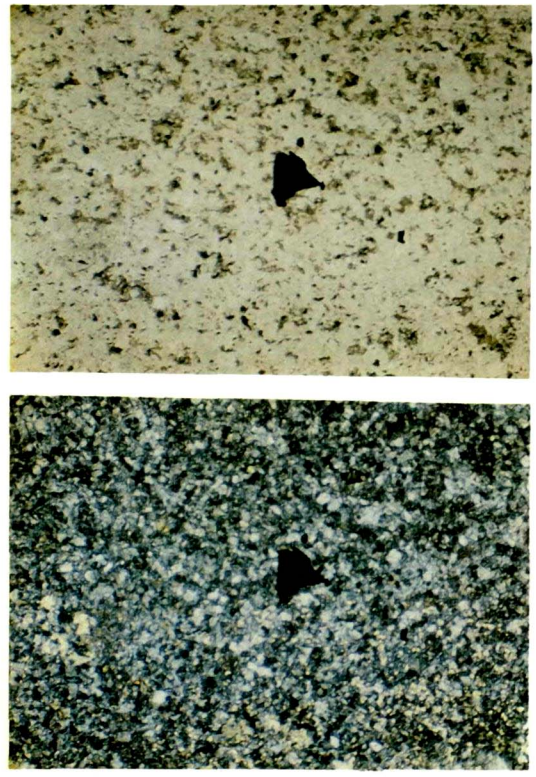

Fig. 12. A photomicrograph of the volcanogenic fine sandstone shows well sorted fine sands to silts, which appears to be partly altered to calacite and clay minerals. Black opaque mineral is pyrite, showing yellowish brown color induced by surface weathering.

The rock is mainly composed of phenocrysts of plagioclase and hornblende and groundmass containing plagioclase laths and little amount of opaque minerals (Fig. 13). The plagioclase phenocryst, 0.5−2.0 cm in long axis, range from intermediate to calcic in composition (labradorite to bytownite) (Fig. 14), suggesting that the rock falls into the category of basaltic andesite porphyry. The field relationship between this porphyry and other rocks is not

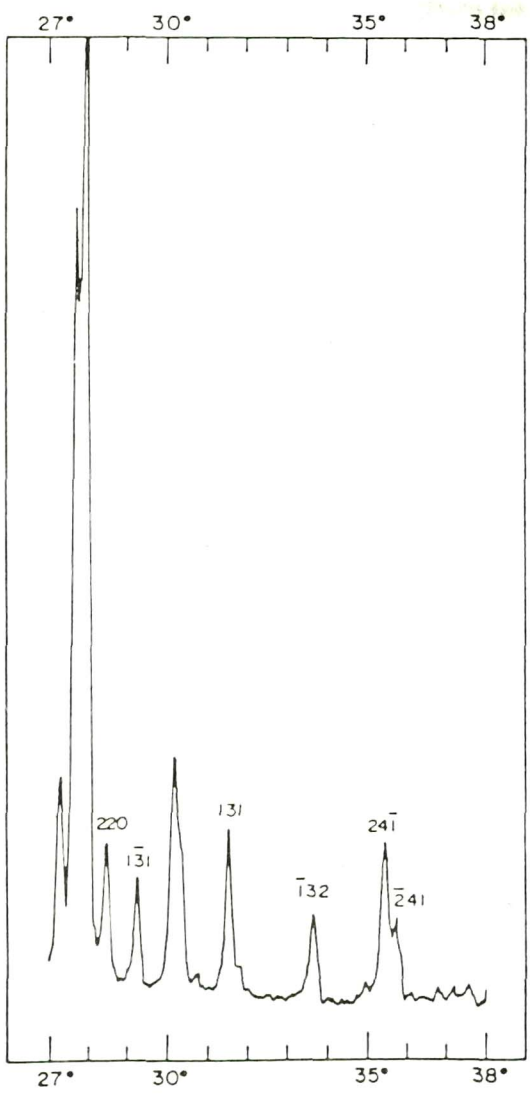

Fig. 13. An X-ray diffractogram of the plagioclase phenocryst shows that it could be a labradorite to bytownite.

clear, because its distribution is limited at beach gravel deposits along the coasts (Fig. 1 and Fig. 15).

6. Quartz-diorite

Previous workers (Barton, 1965; Davies, 1982; Kang and Jin, 1989) have interpreted that quartz-diorite intruded the volcanic rocks

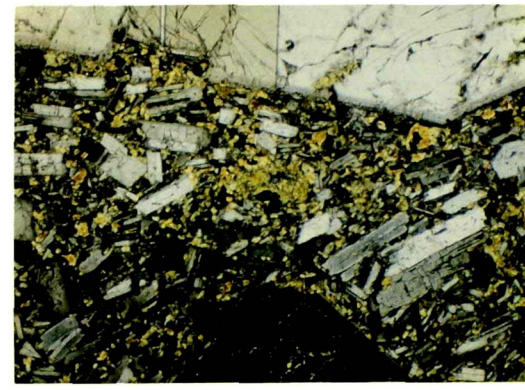

Fig. 14. A photomicrograph of the basaltic andesite porphyry shows labradorite phenocryst(upper black part and lower part) with fine laths and mafic minerals in groundmass (in crossed nicols).

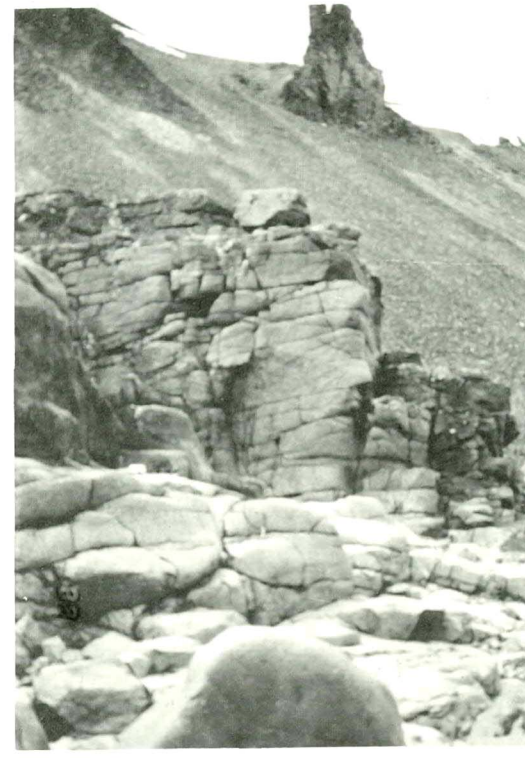

Fig. 15. An outcrop of the basaltic andesite porphyry distributed along the southwestern coast in the Barton Peninsula.

described above. However, the contact between the quartz-diorite and volcanic rocks is rarely seen and uncertain because the boundary is largely covered by the talus of the volcanic rocks at the northern coast, or overlain by beach gravel deposits around the western point.

This quartz-diorite, cropping out along the western and northern coast of the Barton Peninsula, is equigranular in texture and fine grained. In thin section, plagioclase, hornblende, biotite are abundant or common, but interstitial quartz and opaque minerals are also present with secondary minerals such as chlorite, sericite and epidote (Fig. 16).

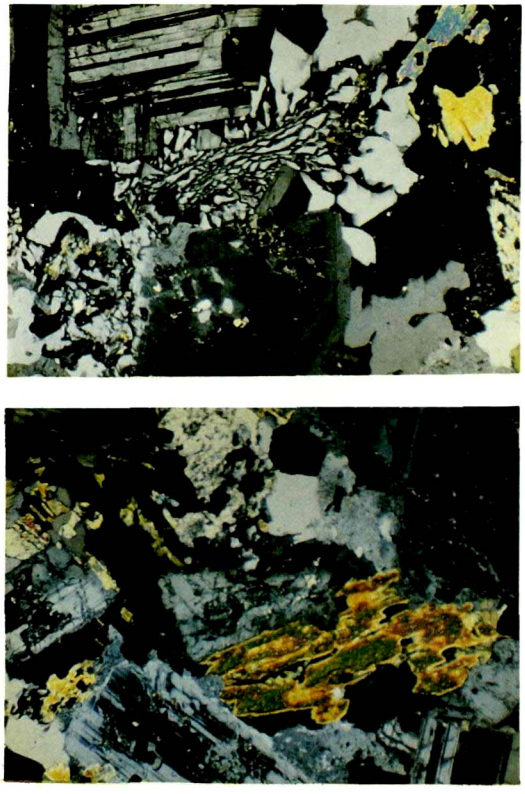

Fig. 16. A photomicrograph of the quartz-diorite shows equigranular and fine grained in texture composed of plagioclase, hornblende, biotite, interstitial quartz and opaque minerals.

Geochemistry

All the volcano-plutonic rocks of the two peninsulas are highly variable in occurence and rock phase. Despite this, the rocks are likely to be derived from a cogenetic magma, based on their association in time and space.

A total of 28 bulk rock samples (Fig. 17) were analyzed for major, trace and rare earths elements using ICP techniques at London University, U.K. CIPW normative minerals are also calculated, based on the analytical data (Table 1).

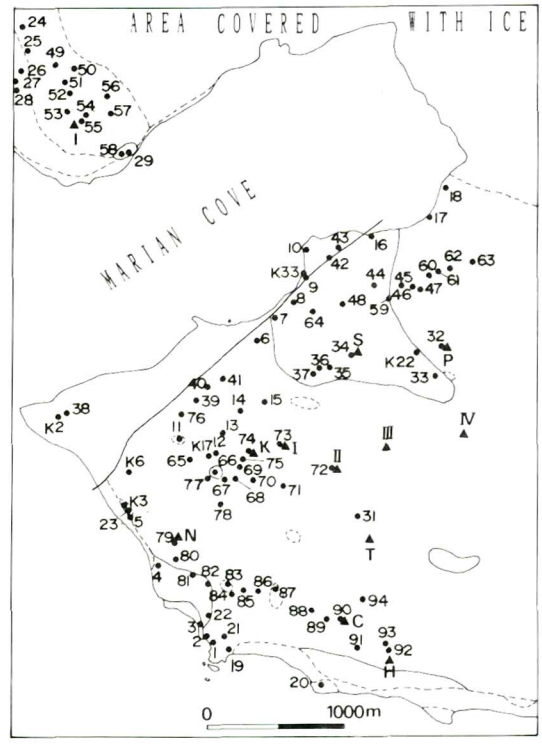

Fig. 17. Location map of the rock samples taken in the Barton and Weaver Peninsulas around the King Sejong Station, ROK.

1. Major element geochemistry

The variations of major elements are plotted

Table 1. Major oxides and CIPW normative minerals for the volcano−plutonic rocks in the Barton and Weaver Peninsula of the King George Island Antarctica.

(in weight percent)

Sample No.	o	o	o	x	#	x	x
elements	7	8	10	14	16	19	25A
SiO_2	55.13	64.60	62.38	52.35	50.14	54.02	54.45
TiO_2	0.70	0.54	0.58	0.68	0.56	1.40	0.76
Al_2O_3	18.42	16.22	16.70	20.87	20.24	16.34	17.66
Fe_2O_3	8.04	5.54	5.96	9.12	7.80	11.45	8.33
MnO	0.16	0.10	0.12	0.19	0.40	0.18	0.14
MgO	4.21	2.15	3.06	4.07	6.18	4.19	2.66
CaO	7.75	4.17	4.76	9.72	8.02	7.63	5.27
Na_2O	4.01	3.86	3.89	3.35	1.66	3.19	4.48
K_3O	1.20	3.03	2.63	0.42	0.45	2.21	2.64
P_2O_5	0.20	0.16	0.18	0.19	0.05	0.39	0.18
total	99.82	100.37	100.26	100.96	95.50	101.00	96.57
Normative Minerals							
Q	2.31	16.22	12.69	1.16	8.57	2.01	0.00
Or	7.15	17.92	15.57	2.47	2.80	13.04	16.26
Ab	34.21	32.68	32.99	28.28	14.80	26.97	39.52
An	28.95	17.99	20.38	40.57	41.58	23.71	21.14
Di	7.01	1.39	1.70	5.23	0.00	9.66	4.11
Hy	16.88	11.25	13.89	18.67	26.34	18.73	15.24
Mt	1.41	0.96	1.03	1.58	1.43	1.99	1.51
Il	1.34	1.02	1.10	1.28	1.12	2.65	1.50
Ap	0.46	0.36	0.41	0.43	0.12	0.89	0.43
Co	0.00	0.00	0.00	0.00	2.70	0.00	0.00
total	99.74	99.83	99.81	99.70	99.48	99.69	99.75
S.I	24.94	15.17	20.24	24.95	39.18	20.77	15.21
D.I	72.63	84.83	81.64	72.49	67.76	65.75	76.94
C.I	27.11	15.00	18.16	27.21	31.71	33.94	22.81
Ka_2O/Na_2O	0.29	0.78	0.67	0.12	0.27	0.69	0.58
Alkali/CaO	0.67	1.65	1.37	0.38	0.26	0.70	1.35
I/S	0.83	0.94	0.93	0.88	1.13	0.75	0.88

(continued)

(in weight percent)

Sample No.	@	#	@	@	*	*	〃
elements	25B	27	31	32	33	37	38
SiO_2	61.61	51.70	56.15	57.69	63.66	62.22	57.52
TiO_2	0.49	0.83	0.76	0.76	0.61	0.65	0.76
Al_2O_3	16.44	16.65	17.95	17.37	16.36	16.71	17.11
Fe_2O_3	5.16	7.35	8.73	8.13	6.06	61385	8.02
MnO	0.09	0.18	0.16	0.14	0.11	0.12	0.14
MgO	1.84	3.62	3.67	3.98	2.33	2.68	3.76
CaO	3.59	6.60	6.72	7.63	4.69	5.23	7.12
Na_2O	3.31	4.07	3.09	3.03	4.19	3.95	3.67
K_3O	3.95	1.59	0.45	0.83	2.77	2.42	1.79
P_2O_5	0.14	0.17	0.21	0.23	0.16	0.16	0.23
total	96.62	92.76	97.89	99.79	100.94	100.52	100.12
			Normative Minerals				
Q	14.95	1.04	12.73	12.00	13.27	12.69	6.70
Or	24.26	10.19	2.73	4.94	16.29	14.30	10.63
Ab	29.11	37.36	26.90	25.86	35.29	33.42	31.21
An	17.57	23.37	32.90	31.61	17.56	20.71	25.05
Di	0.00	8.22	0.00	4.18	3.80	3.48	7.41
Hy	11.16	14.99	20.23	17.72	11.01	12.47	15.35
Mt	0.93	1.38	1.56	1.42	1.04	1.11	1.40
Il	0.96	1.71	1.48	1.45	1.15	1.23	1.45
Ap	0.33	0.42	0.49	0.53	0.36	0.36	0.53
Co	0.00	0.00	0.67	0.00	0.00	0.00	0.00
total	99.84	99.71	99.73	99.76	99.82	99.80	99.76
S.I	13.26	22.43	23.99	25.90	15.63	17.91	22:59
D.I	85.90	72.97	75.27	74.43	82.43	81.13	73.60
C.I	13.94	26.73	24.46	25.33	17.39	18.67	26.15
Ka_2O/Na_2O	1.19	0.39	0.14	0.27	0.66	0.61	0.48
Alkali/CaO	2.02	0.85	0.52	0.50	1.48	1.21	0.76
I/S	1.01	0.81	1.00	0.87	0.88	0.89	0.81

(*continued*)

(in weight percent)

Sample No. elements	* 42	* 44	x 51	+ 58	@ 72	# 76	v 87
SiO_2	66.75	56.26	53.18	54.15	59.63	51.14	63.24
TiO_2	0.47	0.84	0.63	0.62	0.66	0.62	0.90
Al_2O_3	15.82	18.03	19.04	22.37	17.60	18.94	15.43
Fe_2O_3	4.63	8.91	7.39	6.23	6.13	81425	4.62
MnO	0.11	0.17	0.12	0.11	0.15	0.15	0.17
MgO	1.87	3.99	3.70	2.49	2.91	5.94	2.52
CaO	3.55	7.72	8.53	10.18	6.12	10.28	6.01
Na_2O	3.66	3.90	2.78	3.24	2.94	2.69	2.09
K_3O	3.24	0.17	2.13	0.88	3.41	0.25	1.36
P_2O_5	0.13	0.25	0.16	0.18	0.19	0.19	0.32
total	100.23	100.24	97.66	100.45	99.74	95.93	96.66
Normative Minerals							
Q	20.56	7.50	3.28	4.72	10.30	1.86	29.04
Or	19.17	1.00	12.96	5.20	20.30	1.50	8.34
Ab	31.01	33.15	24.23	27.43	25.06	23.24	18.36
An	16.79	31.33	34.18	43.91	24.94	39.68	28.82
Di	0.00	4.57	6.89	4.52	3.64	9.09	0.00
Hy	10.14	18.40	15.28	11.33	12.73	21.21	11.45
Mt	0.80	1.55	1.32	1.08	1.07	1.49	0.83
Il	0.89	1.60	1.23	1.17	1.26	1.20	1.77
Ap	0.29	0.57	0.37	0.41	0.44	0.44	0.76
Co	0.14	0.00	0.00	0.00	0.00	0.00	0.36
total	99.83	99.72	99.79	99.81	99.78	99.75	99.77
S.I	14.29	24.44	23.96	20.11	19.43	35.62	24.38
D.I	87.54	73.01	74.67	81.27	80.61	66.29	84.58
C.I	12.29	26.71	25.11	18.54	19.16	33.45	15.18
Ka_2O/Na_2O	0.88	4.00	0.76	0.27	1.15	9.00	0.65
Alkali/CaO	1.94	0.52	0.57	0.40	1.03	0.28	0.57
I/S	0.98	0.87	0.85	0.90	0.89	0.81	0.97

abbreviations imply as follow :
S.I ; solidification index, D.I ; differentiation index, C.I ; crystallization index, Alkalis ; Na_2O+K_2O, I/S ; $Al_2O_3/(CaO+Na_2O+K_2O)$. o ; quartz−diorite to granodiorite, * ; crystal tuff(dacitic and/or rhyolitic), # ; basaltic tuff, x ; basaltic andesitic tuff, @ ; andesitic tuff, + ; basaltic andesite porphyry, v ; volcanogenic sandsatone with subordinate siltstone.

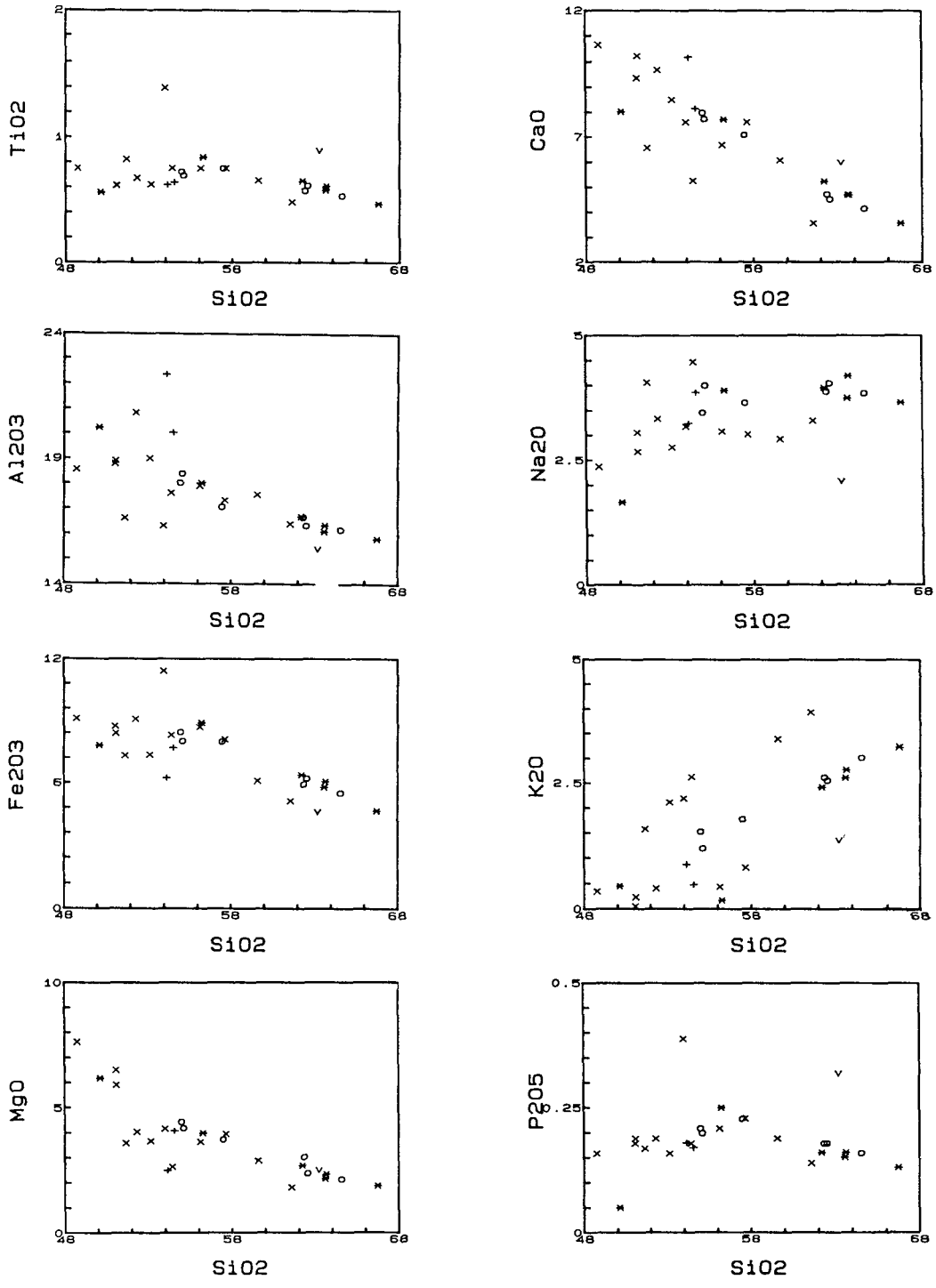

Fig. 18. Harker diagrams for the volcano-plutonic rocks show regular variations with increasing SiO_2 content. (Symbols mean as follows : o, quartz−diorite ; *, crystal tuff ; +, basaltic andesite porphyry ; v, volcanogenic sandstone)

on the Harker's diagram (Fig. 18). Regular variations of interelements are much pronounced except K_2O, suggesting that the volcano-plutonic rocks are fractionally crystallized from a typical calc-alkaline magma.

SiO_2 content for the rocks ranges from basaltic (48 %) through andesitic (58 %) upto acidic (68 %), and TiO_2, Al_2O_3, total Fe_2O_3, MgO, CaO and P_2O_5 contents are decreasing with increasing SiO_2 content except a few data deviated from the main trend, respectively.

In contrast, Na_2O content shows a weak increasing trend with the increasing SiO_2 content, but K_2O content shows a strong fluctuation to the SiO_2 values. This fluctuation, very strong in basaltic composition, appears to be affected by either the later hydrothermal activities which are widely recognized in the Barton Peninsula, or weathering processes of the volcanic rocks on the surface.

In order to define magma type of the rocks, an AFM (Alkalis-total Fe_2O_3/1.1-MgO) diagram is constructed (Fig. 19). All the plots follow a typical trend of hypersthenic series of calc-alkaline magma, as in the Tertiary volcanics from the South Shetland Islands (Tarney et al., 1982), or in the modern magmatic arcs such as the Western American Volcanic arcs and Continental Island arcs (Meijer, 1982). In particular, low content of titanium (ranging from 1.40 to 0.47 %) and high content of alumina (ranging from 22.37 to 15.43 %) of the rocks reflect a calc-alkaline origin.

Alkalis versus SiO_2 diagram (Fig. 20) for the rocks demonstrates that most of the volcano-plutonic rocks also fall in the field of the calc-alkaline (subalkaline) trend (Miyashiro, 1978).

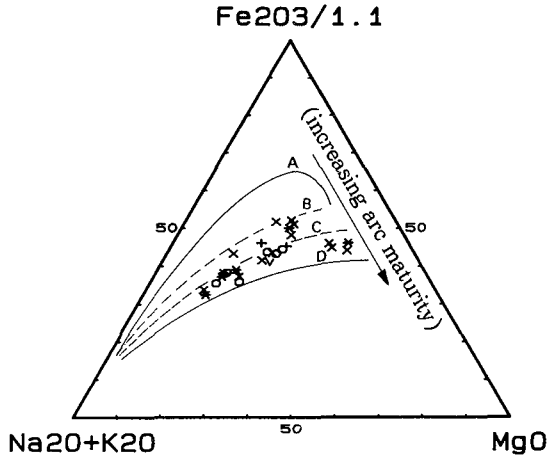

Fig. 19. AFM diagram for the volcano-plutonic rocks shows that all the plots fall into B, C, D field of calc-alkaline magma. The category indicates volcanic rock suites of the modern magmatic arcs as follows : A, Tonga-Mariana-S. Sandwich ; B, Aleutians-Lesser Antilles ; C, New Zealand-Mexico-Japan ; D, Cascade-N. Chile-New Guinea (Meijer, 1982). (Symbols are the same as in Fig. 17)

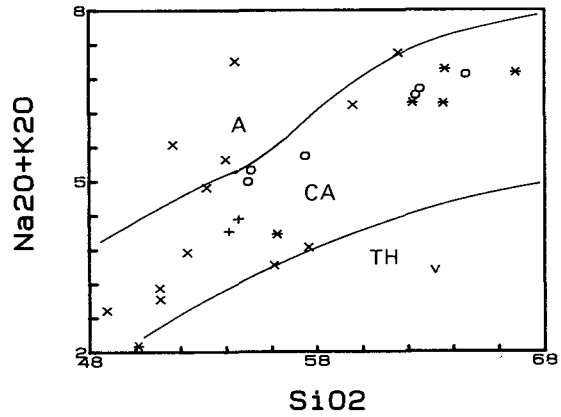

Fig. 20. Plot of total alkalis versus SiO_2 content in weight % for the rocks of the Barton and Weaver Peninsulas around the King Sejong Station. (Symbols are the same as in Fig. 18)

The TiO_2-K_2O-P_2O_5 triangular diagram for the rocks (Fig. 21) shows that they have been differentiated from basaltic to rhyolitic rocks. In addition to these, the SiO_2 versus (Fe_2O_3/1.1)/MgO diagram (Fig. 22) features that the rocks

have a typical calc-alkaline nature.

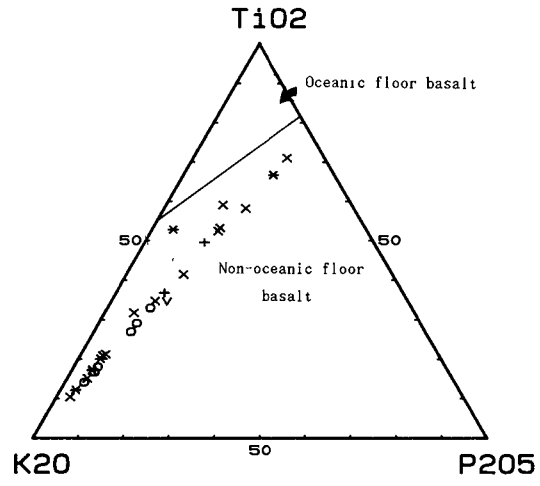

Fig. 21. Triangular diagram of $TiO_2-K_2O-P_2O_5$ for the volcano-plutonic rocks with dividing line between oceanic basalt and non-oceanic basalt fields. (Symbols are the same as in Fig. 18)

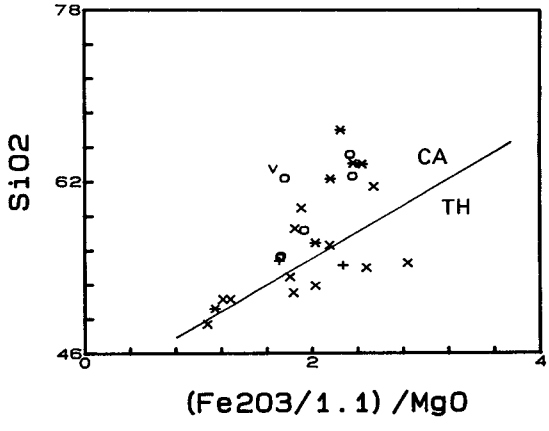

Fig. 22. Plot of SiO_2 against $(Fe_2O_3/1.1)/MgO$ for the rocks in order to distinguish calc-alkaline and tholeiitic rocks around the King Sejong Station. (after Miyashiro, 1974) (Symbols are the same as in Fig. 18)

2. Trace element geochemistry

Analytical data for 26 trace and rare earth elements of the rocks are presented in Table 2.

1) Trace element variation versus SiO_2

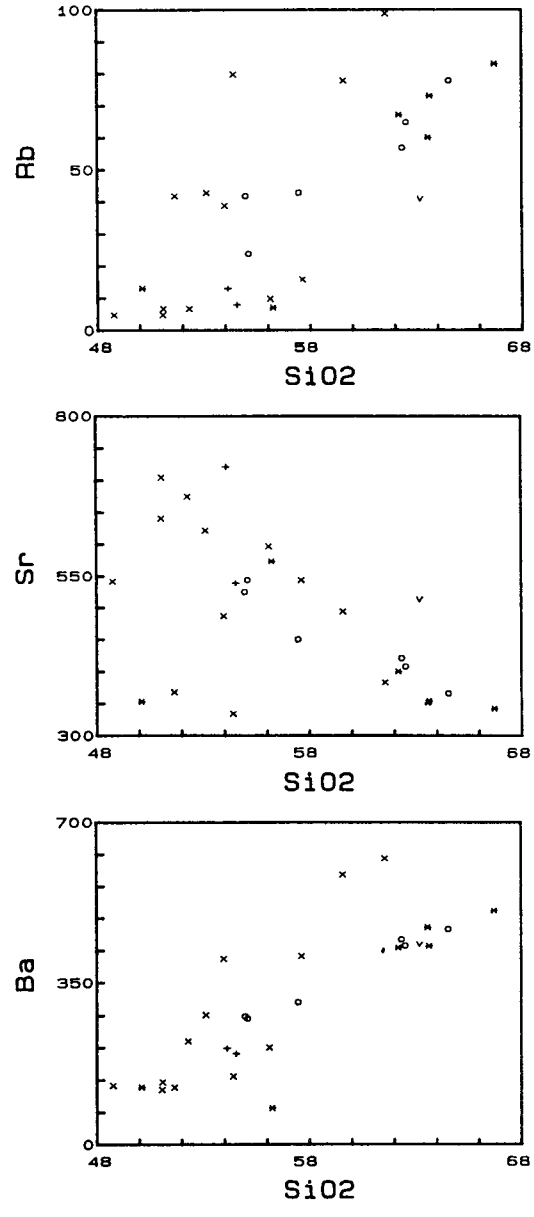

Fig. 23. LIL elements versus SiO_2 variation diagram for the rocks. (Symbols are the same as in Fig. 18)

Table 2. Trace and rare earths element abundance for the volcano-plutonic rocks in the Barton and Weaver Peninsula, the King George Island, Antarctica.

(in parts per millon)

sample No.	o	o	o	x	#	x	x	@	#
elements	7	8	10	14	16	19	25a	25b	27
Ba	275	469	446	226	125	404	150	623	126
Co	23	14	15	22	16	27	19	12	19
Cr	19	18	23	17	45	20	6	10	7
Cu	234	111	72	80	206	315	137	65	152
Li	22	18	19	16	29	19	25	29	40
Nb	3	5	4	2	4	5	2	4	2
Ni	20	16	16	16	28	20	13	12	11
Rb	24	78	57	7	13	39	80	99	42
Sc	23	13	17	23	21	34	24	13	24
Sr	545	367	422	676	353	488	335	384	369
V	205	113	136	218	148	325	230	108	195
Y	22	27	27	14	14	33	15	19	18
Zn	144	64	62	58	177	101	81	55	78
Zr	65	142	130	42	39	115	50	114	53
				Rare Earth Elements					
La	14.20	22.00	20.50	7.90	11.50	21.60	9.70	16.90	9.20
Ce	32.92	50.52	47.55	18.42	24.97	48.54	22.71	37.48	21.50
Pr	4.38	6.30	5.98	2.49	3.03	6.40	3.08	4.67	3.09
Nd	19.90	26.40	25.40	12.10	13.30	29.80	14.50	19.90	15.10
Sm	4.30	5.46	5.36	2.69	2.61	6.60	3.35	4.07	3.48
Eu	1.28	1.15	1.20	1.04	1.00	1.79	1.13	0.94	1.25
Gd	4.27	5.03	4.98	2.92	2.52	6.68	3.44	3.91	3.89
Dy	3.67	4.44	4.42	2.53	2.32	5.99	3.03	3.49	3.47
Ho	0.67	0.83	0.82	0.46	0.44	1.11	0.57	0.66	0.65
Er	2.08	2.50	2.46	1.41	1.57	3.16	1.67	1.99	1.96
Yb	2.00	2.51	2.43	1.27	1.76	2.94	1.58	1.99	1.79
Lu	0.30	0.40	0.39	0.20	0.26	0.45	0.25	0.32	0.28
ΣREE	89.97	127.54	121.49	53.43	64.98	135.06	65.01	96.32	65.66
La/Sm	3.30	4.03	3.82	2.94	4.41	3.27	2.90	4.15	2.64
La/Yb	7.10	8.76	8.44	6.22	6.53	7.35	6.14	8.49	5.14
Eu/Sm	0.30	0.21	0.22	0.39	0.38	0.27	0.33	0.23	0.36
Eu/Eu	0.90	0.66	0.70	1.12	1.18	0.92	1.01	0.71	1.04
$(La/Lu)_{CN}$	4.91	5.71	5.46	4.10	4.59	4.98	4.03	5.48	3.41
$(Gd/Lu)_{CN}$	1.77	1.56	1.59	1.81	1.20	1.85	1.71	1.52	1.73

(continued)

(in parts per millon)

sample No.	@	@	*	*	o	*	*	x	+
elements	31	32	33	37	38	42	44	51	58
Ba	212	410	430	426	310	507	80	283	209
Co	24	22	15	16	21	12	24	20	16
Cr	22	25	16	15	15	11	26	31	10
Cu	41	145	45	93	112	32	6	93	131
Li	20	26	28	25	18	12	21	18	11
Nb	4	5	5	5	5	4	3	3	2
Ni	20	24	15	16	19	12	21	18	11
Rb	10	16	73	67	43	83	7	43	13
Sc	23	24	14	17	24	10	27	22	18
Sr	598	545	354	400	451	342	573	623	721
V	190	210	126	150	203	90	233	193	182
Y	19	22	27	26	26	25	24	17	14
Zn	87	35	52	71	54	61	90	64	61
Zr	106	103	132	122	135	122	101	77	54
Rare Earth Elements									
La	17.90	18.00	20.40	18.70	21.40	22.40	18.80	11.60	8.80
Ce	42.58	41.17	48.03	43.23	50.42	50.42	43.96	25.52	20.35
Pr	5.63	5.36	6.11	5.43	6.12	6.12	5.79	3.33	2.82
Nd	25.60	24.40	26.30	23.50	25.50	25.50	26.30	15.20	13.40
Sm	5.62	5.28	5.51	5.08	5.16	5.16	5.76	3.24	2.99
Eu	1.44	1.33	1.19	1.15	1.05	1.05	1.54	1.03	1.05
Gd	5.33	4.96	4.98	4.86	4.66	4.66	5.43	3.29	3.18
Dy	4.34	4.10	4.61	4.43	4.13	4.13	4.42	2.82	2.66
Ho	0.79	0.74	0.86	0.83	0.78	0.78	0.79	0.53	0.49
Er	2.22	2.11	2.52	2.45	2.27	2.27	2.21	1.53	1.50
Yb	2.04	1.96	2.59	2.49	2.37	2.37	2.07	1.44	1.34
Lu	0.32	0.30	0.40	0.39	0.38	0.38	0.32	0.23	0.21
ΣREE	113.81	109.71	123.50	112.54	128.32	125.24	117.39	69.76	58.79
La/Sm	3.19	3.41	3.70	3.68	3.58	4.34	3.26	3.58	2.94
La/Yb	8.77	9.18	7.88	7.51	9.22	9.45	9.08	8.06	6.57
Eu/Sm	0.26	0.25	0.22	0.23	0.23	0.20	0.27	0.32	0.35
Eu/Eu	0.79	0.79	0.69	0.70	0.72	0.64	0.83	0.96	1.03
$(La/Lu)_{CN}$	5.81	6.23	5.30	4.98	6.17	6.12	6.10	5.23	4.35
$(Gd/Lu)_{CN}$	2.13	2.05	1.55	1.55	1.91	1.52	2.11	1.78	1.88

(continued)

(in parts per millon)

sample No.	@	#	v	o	+	#	#	*	o
elements	72	76	87	K2	K3	K6	K17	K22	K33
Ba	588	137	435	280	197	121	130	471	432
Co	16	25	13	21	20	26	32	14	15
Cr	19	59	9	19	36	95	96	11	15
Cu	71	83	93	92	66	88	69	86	89
Li	14	14	23	18	9	8	11	16	17
Nb	5	3	4	4	2	2	3	4	5
Ni	18	35	9	21	24	46	69	13	13
Rb	78	7	41	42	8	5	5	60	65
Sc	17	26	21	27	20	29	27	16	14
Sr	495	706	514	526	539	642	543	351	409
V	141	212	126	212	170	220	215	138	137
Y	23	13	23	23	15	14	14	27	30
Zn	50	72	67	73	76	62	62	69	66
Zr	150	37	112	120	52	41	41	129	107
Rare Earth Elements									
La	24.70	14.00	18.50	19.00	7.80	14.50	9.20	18.30	21.20
Ce	54.47	31.20	46.51	43.85	18.13	32.54	20.38	42.50	49.33
Pr	6.85	3.98	6.26	5.63	2.58	4.13	2.72	5.59	6.29
Nd	29.20	18.40	28.30	25.10	12.10	19.20	12.90	23.80	27.40
Sm	5.92	3.81	6.27	5.31	2.64	4.03	2.74	5.13	5.94
Eu	1.30	1.23	1.57	1.31	1.01	1.35	0.94	1.13	1.25
Gd	5.35	3.50	5.94	5.02	3.09	3.83	2.97	5.07	5.53
Dy	4.42	2.64	4.88	4.23	2.71	3.02	2.60	4.51	4.97
Ho	0.80	0.47	0.88	0.78	0.52	0.54	0.49	0.86	0.92
Er	2.29	1.31	2.47	2.23	1.57	1.54	1.45	2.57	2.68
Yb	2.18	1.15	2.35	2.10	1.43	1.38	1.27	2.53	2.65
Lu	0.33	0.17	0.37	0.33	0.23	0.21	0.20	0.40	0.41
ΣREE	137.81	81.86	124.30	114.89	53.81	86.27	57.86	112.39	128.57
La/Sm	4.17	3.67	2.95	3.58	2.95	3.60	3.36	3.57	3.57
La/Yb	11.33	12.17	7.87	9.05	5.45	10.51	7.24	7.23	8.00
Eu/Sm	0.22	0.32	0.25	0.25	0.38	0.33	0.34	0.22	0.21
Eu/Eu	0.69	1.02	0.78	0.77	1.08	1.04	1.00	0.67	0.66
$(La/Lu)_{CN}$	7.77	8.54	5.19	5.98	3.52	7.17	4.77	4.75	5.37
$(Gd/Lu)_{CN}$	2.01	2.56	2.00	1.89	1.67	2.27	1.85	1.58	1.68

abbreviations imply as follow :
O ; quartz-diorite to granodiorite, * ; crystal tuff(dacitic and/or rhyolitic), # ; basaltic tuff, x ; basaltic andesitic tuff, @ ; andesitic tuff, + ; basaltic andesite porphyry, v ; volcanogenic sandsatone with subordinate siltstone.

Large ion lithophile (LIL) elements, Rb, Sr and Ba, show very regular variations with increasing SiO_2 content, respectively (Fig. 23), suggesting that the rocks have been fractionated from a calc-alkaline magma. High field strength (HFS) elements, Zr, Nb and Y, also demonstrate regularly increasing trends with increasing SiO_2 content (Fig. 24), strongly supported that the rocks have a calc-alkaline affinity.

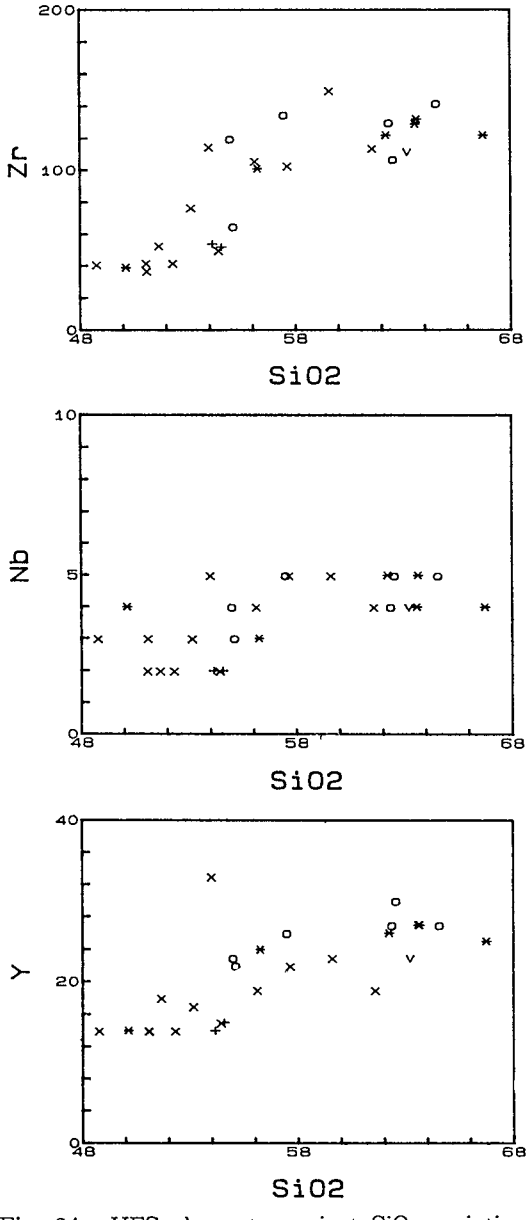

Fig. 24. HFS elements against SiO_2 variation diagram for the rocks. (Symbols are the same as in Fig. 18)

In addition, the transition elements, Ni, V, Sc and Cr, consistently show decreasing trends with increasing SiO_2 content (Fig. 25). Particularly both Ni and Cr for the rocks show exactly the same geochemical chacteristics in that they deplete logarithmically in response to increasing SiO_2. This may reflect their known strong partitioning into olivine and clinopyroxene respectively, and indicated that more olivine and clinopyroxene fractionation had occurred in the basaltic rocks than in dacitic or quartz-dioritic rocks as recognized in thin section study. This implies that the rock suite might belong to a typical calc-alkaline magmatic arc or island arc system.

Furthermore, some of rare earth elements, La, Nd, Eu and Yb, against the SiO_2 diagram are also constructed (Fig. 26). La, Nd and Yb content for the rocks are gradually increasing with increasing SiO_2 content, while conversely Eu content tends to enrich more or less in basaltic to andesitic rocks, and then to deplete in dacitic to rhyolitic (granodioritic) rocks. That is compelling evidence that they have been fractionally crystallized from a calc-alkaline magma.

2) Major and trace elements concerning the tectonic setting

The Ti against Zr diagram (Fig. 27) for the rocks shows that most of the rocks are plotted in low-K tholeiite and/or calc-alkaline fields (Pearce and Cann, 1973). In addition, the Ti-Zr-3Y (Fig. 28) and Ti-Zr-Sr/2 triangular diagram (Fig. 29) for them demonstrate that most of the rocks fall in the low-K tholeiite and/or calc-alkaline fields (Pearce and Cann, 1973).

The CaO versus Y diagram (Fig. 30) indicates that the rocks have been formed from a calc-alkaline magma (Lambert and Holland, 1974).

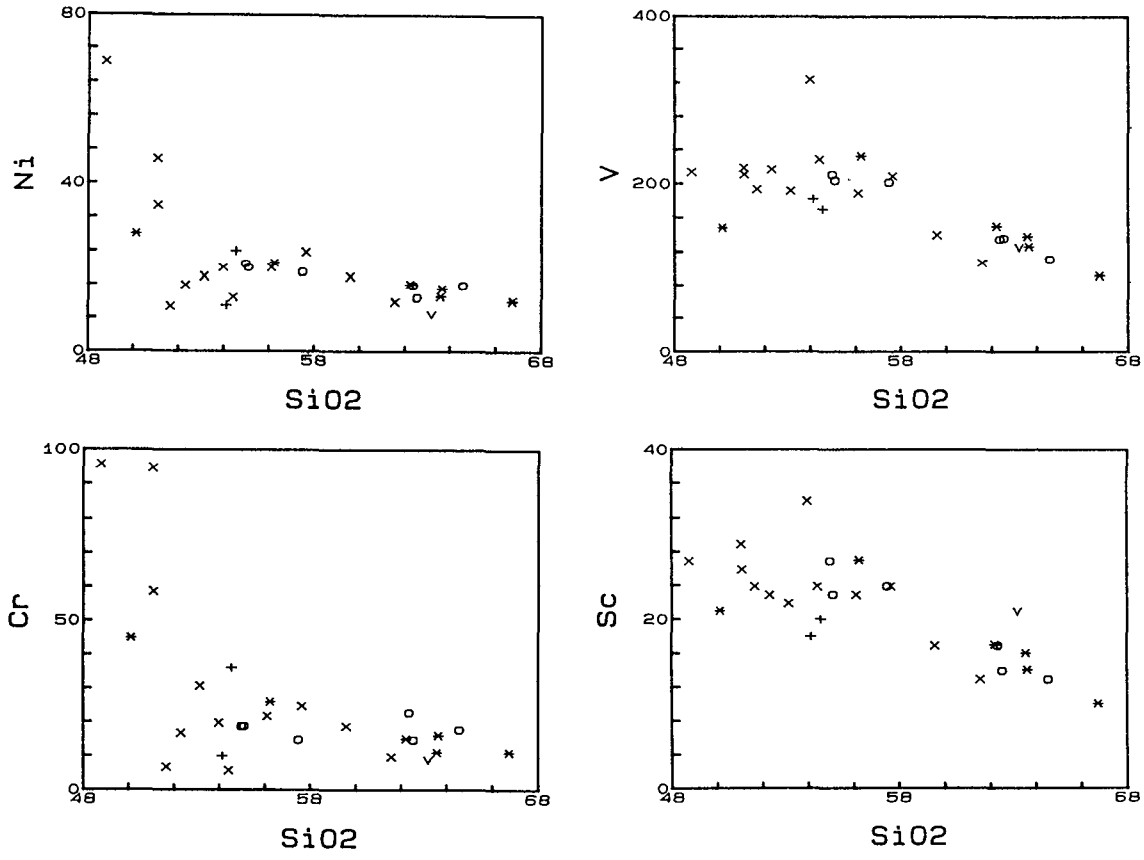

Fig. 25. Transition elements versus SiO_2 variation diagram for the rocks. (Symbols are the same as in Fig. 18)

Additionally, both the Ni versus SiO_2 and Co versus SiO_2 diagrams (Figs. 31 and 32) imply that the rocks have been fractionally crystallized at an island or a magmatic arc environment over the subduction zone (Shoji and Kaneda, 1980).

3) Rare Earth Element (REE) Variation

Total REE (ΣREE) content for the volcano-plutonic rocks range from 53.43 ppm of the basaltic rocks to 137.81 ppm of the rhyolitic rocks with an average of 98.93 ppm (Table 3). The mean ΣREE content for the rocks show an increasing trend with differentiation increased from the basaltic andesite porphyry (56.30 ppm), the basaltic tuff (71.29 ppm at 48−52 % of SiO_2), the basaltic andesitic tuff (80.82 ppm at 52−56 % of SiO_2), andesitic tuff (114.41 ppm at 56−63 % of SiO_2) through the crystal tuff (118.21 ppm) to the granodiorite (118.46 ppm), respectively, on the basis of classification of volcanic rocks by silica content (Fig. 33).

Similarly, the enrichment of the LREE (La/Sm=2.95−3.73) and the slope of the REE pattern, LREE/HREE (La/Yb=6.01−9.44 or La/Lu = 3.94−6.32) are gradually increased with

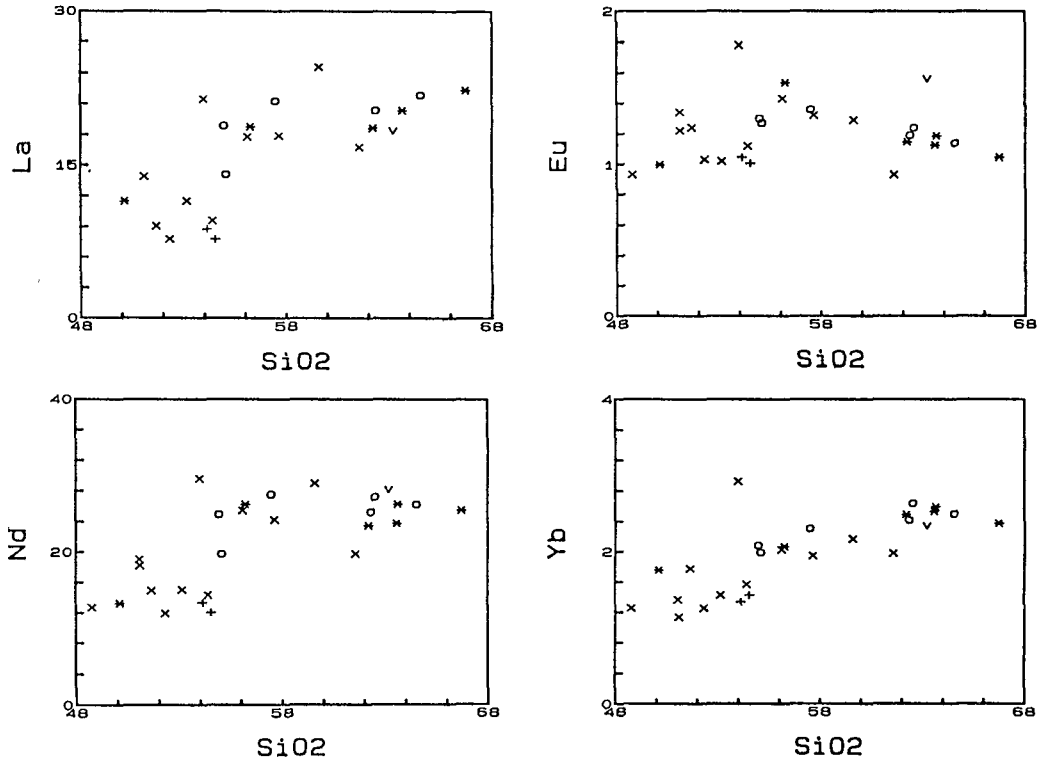

Fig. 26. REE against SiO_2 variation diagram for the rocks. (Symbols are the same as in Fig. 18)

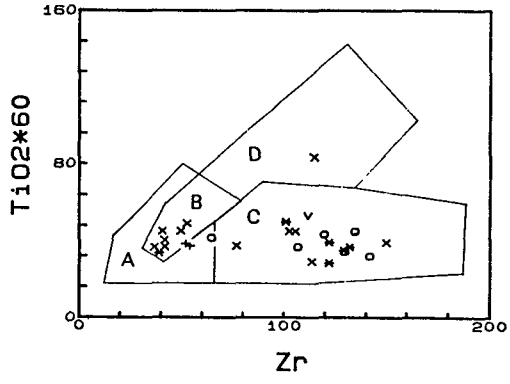

Fig. 27. Discrimination diagram using Ti and Zr in ppm. Ocean−floor basalts (OFB) plot in fields D and B ; lower −potassium tholeiites (LKT) in fields A and B ; and calc−alkaline basalts (CAB) in fields B and C. (after Pearce and Cann, 1973) (Symbols are the same as in Fig. 17)

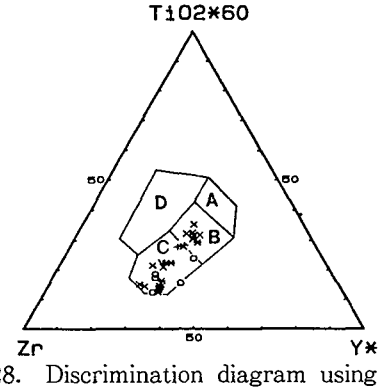

Fig. 28. Discrimination diagram using Ti, Zr and Y in ppm. "Within−Plate" basalt (WPB), i.e., ocean island or continental basalts plot in field D ; ocean −floor basalt (OFB) in field B ; lower−potassium tholeiite (LKT) in fields A and B ; calc−alkaline basalts (CAB) in fields B and C (after Pearce and Cann, 1973) (Symbols are the same as in Fig. 18)

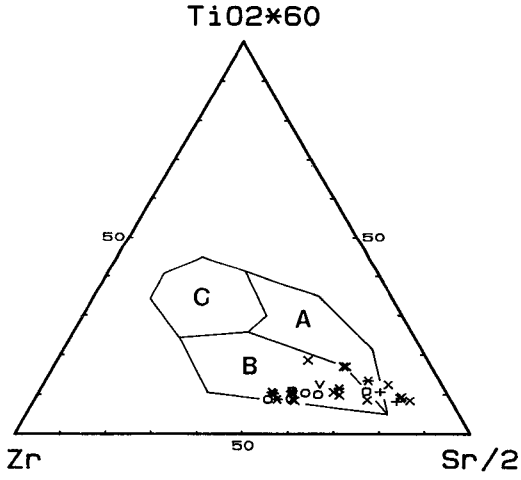

Fig. 29. Discrimination diagram using Ti, Zr and Sr in ppm. Ocean−floor basalts (OFb) plot in field C ; low−potassium tholeiites (LKT) in field A, and calc−alkaline basalts (CAB) in field B (after Pearce and Cann, 1973) (Symbols are the same as in Fig. 18).

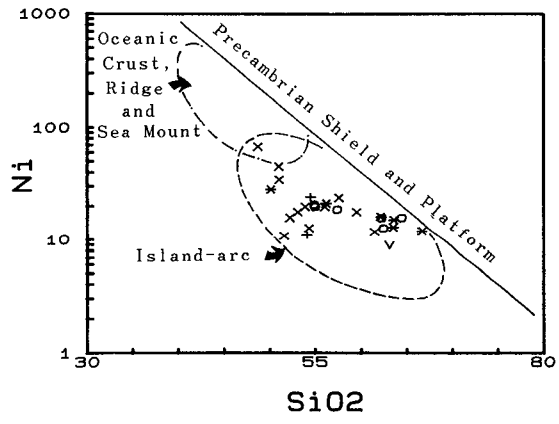

Fig. 31. Discrimination diagram using SiO_2−log Ni plot for the rocks. The soild line, indicating the boundary between the continental type igneous rocks (upper part) and oceanic type igneous rocks (lower part) (after Shoji and Kaneda, 1980) (Symbols are the same as in Fig. 18).

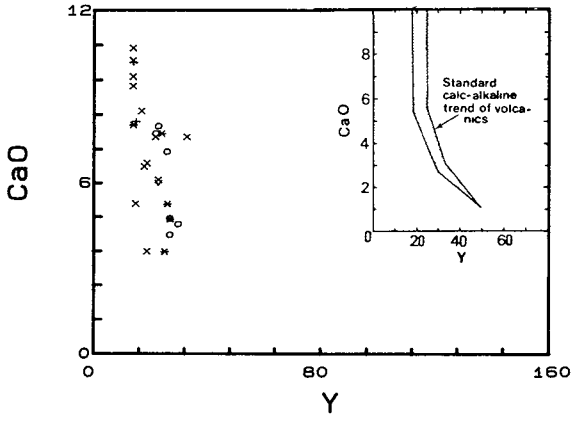

Fig. 30. CaO in weight % and Y in ppm for the rocks. Standard calc−alkaline trend of Lambert and Holland (1974) shown shaded. (Symbols are the same as in Fig. 18).

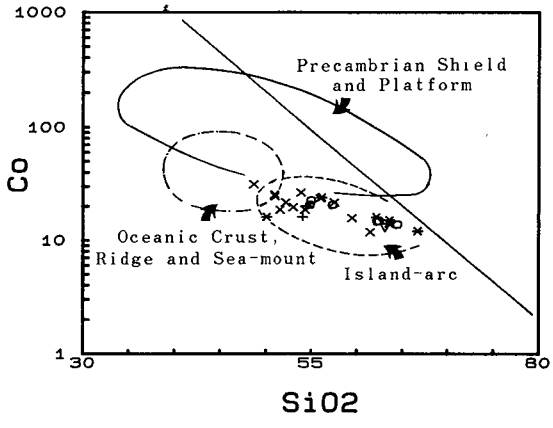

Fig. 32. Discrimination diagram using SiO_2−log Co plot for the rocks. The soild line is the same as in Fig. 31. (after Shoji and Kaneda, 1980) (Symbols are the same as in Fig. 18)

Table 3. The range and mean values of the total REE and various ratios of the REE for each of the volcano-pultonic rock types at the Barton and Weaver Peninsula, King George Island, Antarctica.

rock type	number of samples	Σ REE		La/Sm		La/Yb		Eu/Sm		Eu/Eu*		$(La/Lu)_{CN}$		$(Gd/Lu)_{CN}$	
		range	mean	range	mean	range	mean	range	mean	range	mean	range	mean	range	mean
Basaltic andesite porphyry	2	53.81–58.79	56.30	2.94–2.95	2.95	5.45–6.57	6.01	0.35–0.38	0.37	1.03–1.08	1.06	3.52–4.35	3.94	1.68–1.88	1.78
Volcanic Sandstone	1		124.30		2.95		7.87		0.25		0.78		5.19		2.00
Basaltic tuff	5	57.86–86.27	71.29	2.64–4.41	3.54	5.14–12.17	8.32	0.32–0.38	0.35	1.00–1.18	1.06	3.41–8.54	5.70	1.20–2.56	1.92
Basaltic andesitic tuff	4	53.43–135.06	80.82	2.90–3.58	3.17	6.14–8.06	6.94	0.27–0.39	0.33	0.92–1.12	1.00	4.03–5.23	4.59	1.71–1.85	1.79
Andesitic tuff	4	96.32–137.81	114.41	3.19–4.17	3.73	8.49–11.33	9.44	0.22–0.26	0.24	0.69–0.79	0.75	5.48–7.77	6.32	1.52–2.13	1.93
Crystal tuff	5	112.39–125.24	118.21	3.26–4.34	3.71	7.23–9.45	8.23	0.22–0.27	0.23	0.64–k0.83	k0.71	4.75–6.12	5.45	1.52–2.11	1.66
Grano–diorite	6	89.97–128.57	118.46	3.30–4.03	3.65	7.10–9.22	8.43	0.21–0.30	0.24	0.66–0.90	0.64	4.90–6.17	5.60	1.56–1.91	1.73

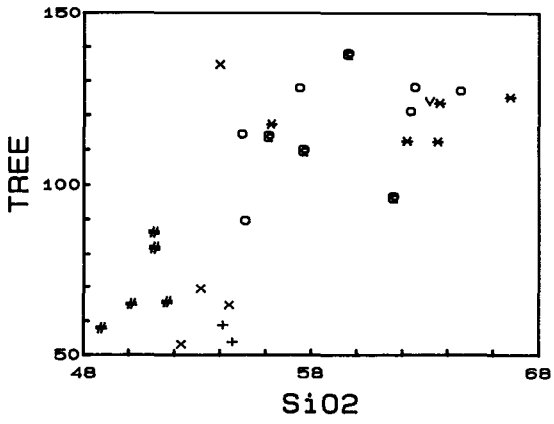

Fig. 33. A plot for the silica content against total REE ($\sum$REE) abundance of the volcano−plutonic rocks.

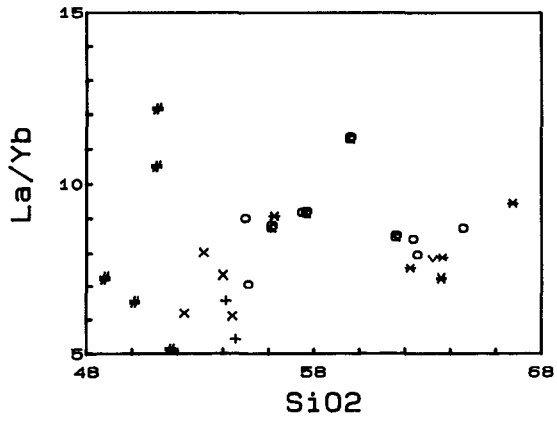

Fig. 35. A plot for the La/Yb against SiO_2 of the rocks.

differentiation of the magma (Fig. 34 and 35). In addition to these, weak positive Eu anomalies (Eu/Eu* > 1) in the basaltic rocks and weak negative Eu anomalies (Eu/Eu* < 1) can be seen in more felsic rocks than the basaltic ones (Fig. 36). Those facts indicate that a magmatic fractional crystallization has occurred.

Chondrite-normalized plots are presented for all the samples in Fig. 37a to 37f, using the C.I. values of Evensen et al. (1978). The six plots represent the seven igneous rock phases of the rocks in an evolutionary sequence (i.e., the ba-

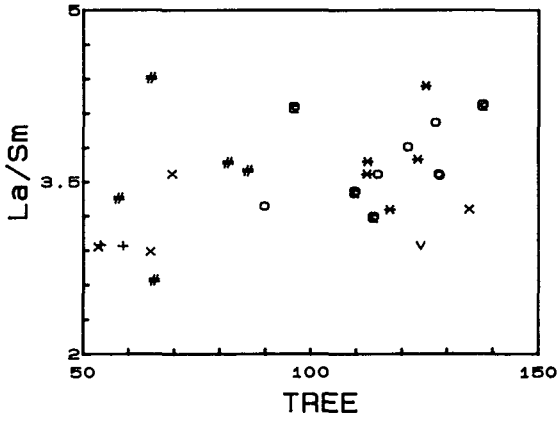

Fig. 34. A plot for the LREE enrichment versus TREE(Total REE, $\sum$REE) of the rocks.

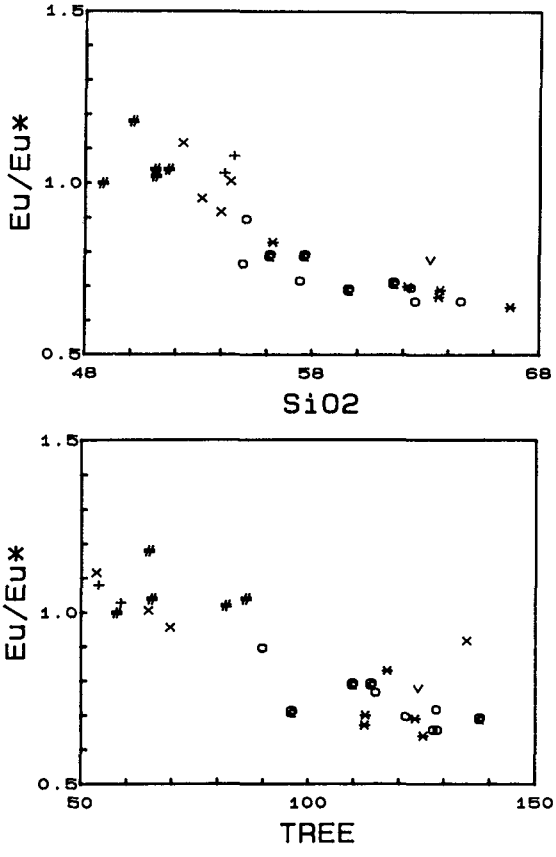

Fig. 36. The correlations between the Eu/Eu* and silica content(A), and Eu/Eu* and TREE(Total REE, $\sum$REE) (B).

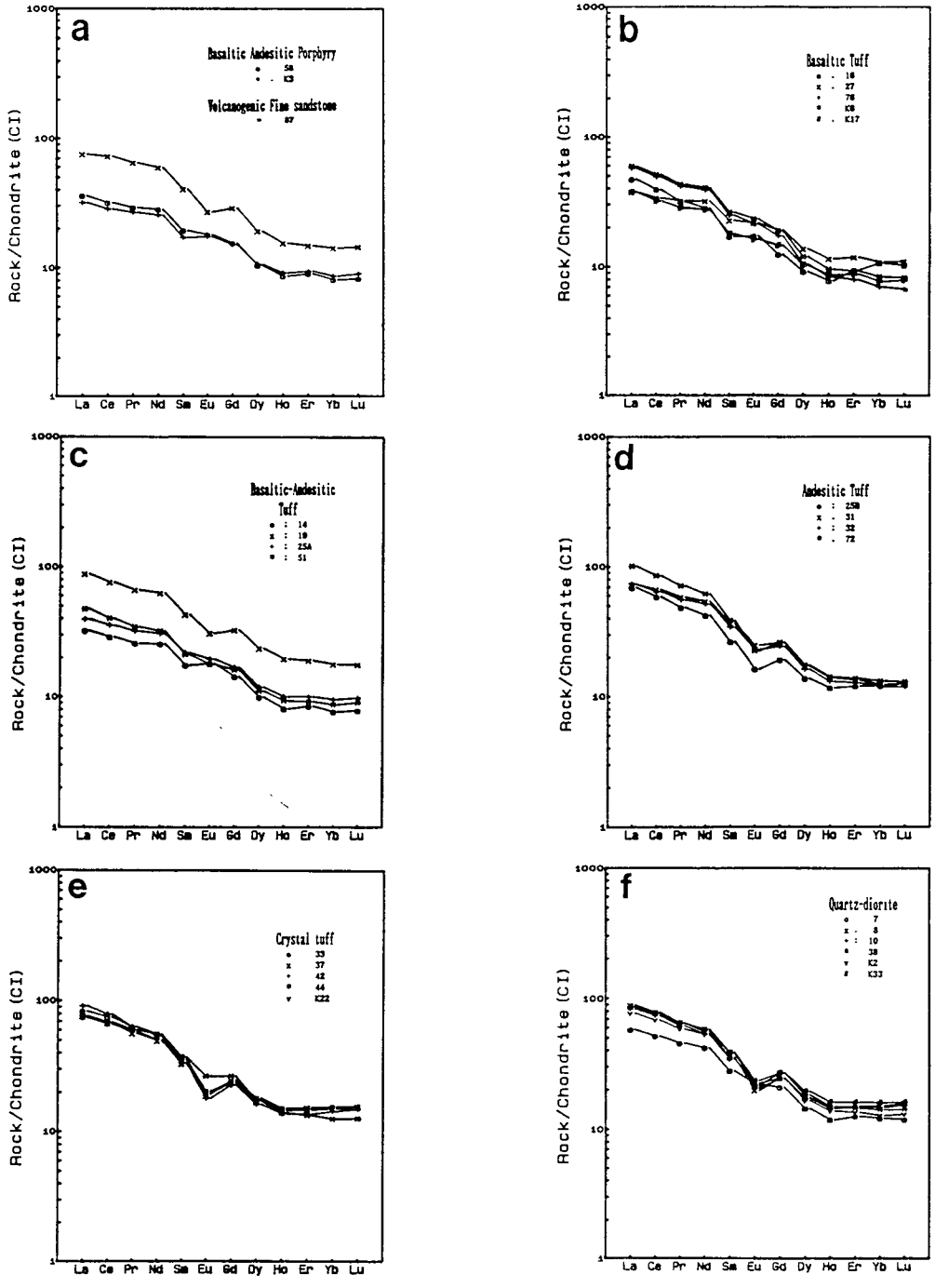

Fig. 37. Chondrite normalized plots for 12 REE of each of the six petrological units in the study area. Values are normalized to those of Evensen et al., (1978). (a) basaltic andesite porphyry and volcanic sandstone, (b) basaltic tuffs, (c) basaltic andesitic tuffs, (d) andesitic tuffs, (e) crystal tuffs, (f) quartz−diorite and granodiorites.

saltic andesite porphyry and the volcanogenic sandstone, the basaltic tuff, the basaltic andesitic tuff, the andesitic tuff, the crystal tuff, and quartz-diorite or granodiorite).

In relation to genesis, the abundance of ΣREE and normalized pattern of REE of the volcanogenic sandstone show the same trend as in the volcano-plutonic rocks mentioned before (Table 3 and Fig. 37a), strongly supporting that the sandstone was formed by acidic volcanic sediments such as crystal tuffs.

The narrowest range of the ΣREE is from 53.81 to 58.79 ppm in the basaltic andesite porphyry, and the widest one is from 53.43 ppm to 135.06 ppm in the basaltic andesitic rocks (Fig. 37c, 38a and 38b). However, there are some difficulties to interpret the REE pattern in the latter. The sample (No. 19) shows not only a typical REE pattern of very evolved rocks as in the crystal tuff or granodioritic rocks but also an erratic higher abundance of total Fe_2O_3 and K_2O than those in normal basaltic andesitic rocks (Table 1 and Table 3). Therefore it could be interpreted that the rock might be initially highly evolved rock, and altered and enriched in those elements and then the silica content relatively resulted in depletion.

The range of the REE pattern of the basaltic rocks is the widest one if the sample (No. 19) were excluded in the basaltic andesitic rocks (Fig. 37d). The fact indicates that the basaltic rocks including basaltic andesitic rocks have much more diverse differentiation than any other rock phases (Fig. 38a).

In particular, the ΣREE abundances and the REE patterns for the crystal tuff and granodiorite show almost the same abundance and trend, suggesting a close relationship of their geneses in terms of temporal, spatial and compositional senses (Fig. 37e and 37f and Fig. 38b).

In addition, the REE pattern of the quartz-dioritic rock is deviated far from those of the granodioritic ones. The pattern is very similar to those of the basaltic to andesitic rocks, reflecting that the rock has been differentiated from quartz-diorites in margin to granodiorite inwards (Fig. 38b).

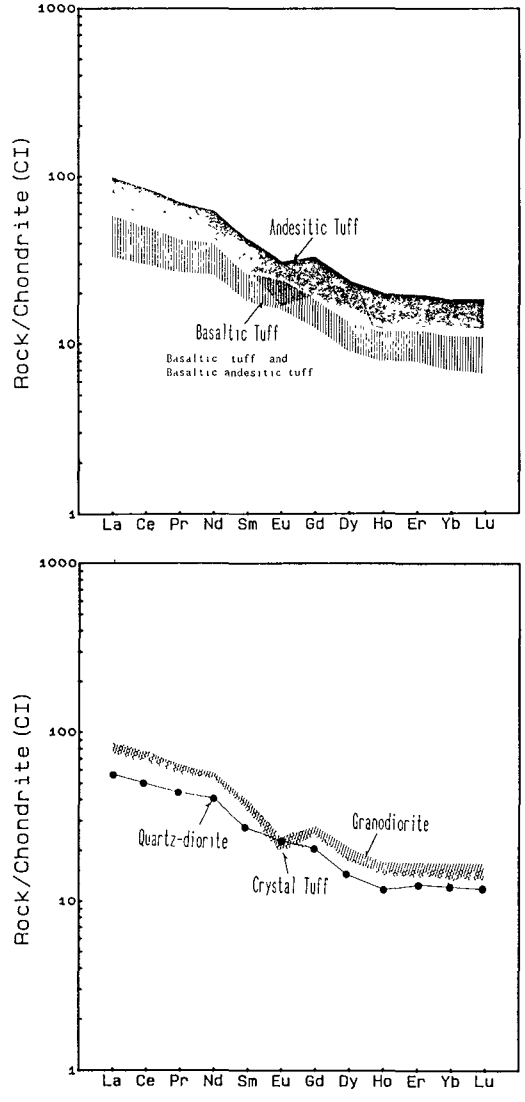

Fig. 38. (a) Composite REE pattern for the basaltic rocks and andesite rocks, (b) Composite REE pattern for the crystal tuffs and granodiorites.

Discussion and Conclusion

As stated in the petrology, the volcano-plutonic rocks distributed in the Barton and Weaver Peninsulas of the King George Island, Antarctica range in composition from basaltic, basaltic andesitic through andesitic to dacitic or quartz-dioritic rocks.

In addition, major and trace element geochemistry including REE for the rocks strongly support that they have been fractionated from a calc-alkaline magma.

With respect to the isotopic age of the rocks, several articles have been published so far. Watt (1982) reported that the K-Ar whole rock age of the granodiorite is 47-52 Ma from Noel Hill, but the age can not be understood. Because the granodiorite was recently recognized as andesitic tuff by Kang and Jin (1989) and Jin et al. (1989), and so the dated rock sample is ambiguous whether it is granodiorite or andesitic tuff. Furthermore, Smellie et al. (1984) dated the lava from Marian Cove by K-Ar whole rock method, which gives 42−48 Ma.

In contrast, Kang and Jin (1989) dated granodiorite in the Barton Peninsula by the Rb-Sr whole rock and biotite two point isochron method and K-AR biotite mothod. The age of it is 63 Ma and 62 Ma, respectively, and the $^{87}Sr/^{86}Sr$ initial ratio is 0.7067. However, Park(1989) also dated five tuffs and a granodiorite sample by K-AR whole rock method, and the ages of them range from 35 Ma to 48 Ma (Table 4).

Table 4. Age data for the volcano-plutonic rocks in the Barton Peninsula.

sample No.	rock type	method	mineral/ whole rock	age (in Ma)	reference
K−34	quartz-diorite	Rb-Sr	biotite	63.4±4.3	Kang and Jin, 1989
K−34	quartz-diorite	K-Ar	whole rock	62.1±1.6	Kang and Jin, 1989
A	tuff	K-Ar	whole rock	48.5±4.0	Park, 1989
B	crystal tuff	K-Ar	whole rock	45.2±1.9	Park, 1989
C	crystal tuff	K-Ar	whole rock	42.1±1.9	Park, 1989
D	quartz-diorite	K-Ar	whole rock	45.2±2.4	Park, 1989
E	tuff	K-Ar	whole rock	35.5±3.4	Park, 1989
F	tuff	K-Ar	whole rock	44.2±2.4	Park, 1989

Consequently, there are two age groups. One is 42−49 Ma, and the other is 62−63 Ma. However, the two granodiorite samples taken in almost same area near to the King Sejong Station yield 62 and 45 Ma, respectively (Kang and Jin, 1989; Park, 1989). Therefore, the younger group might be interpreted as to be affected by the later alterations and mineralizations widely developed in the Barton Peninsula.

In relation to petrogensis of the volcano-plutonic rocks, an ACF (Al_2O_3-Na_2O-K_2O)-CaO-(FeO+MgO) diagram was constructed to define the origin of the magma by the major element data (Fig. 39). Most of the data were plotted in the field of igneous or mantle source. In addition to this, the $^{87}Sr/^{88}Sr$ initial ratio is 0.7067, less than 0.708, suggesting an igneous origin.

Acknowledgements

The authors are deeply indebted to KIER and KORDI, for giving them the honourable opportunity to join the 2nd Korean Antarctic Re-

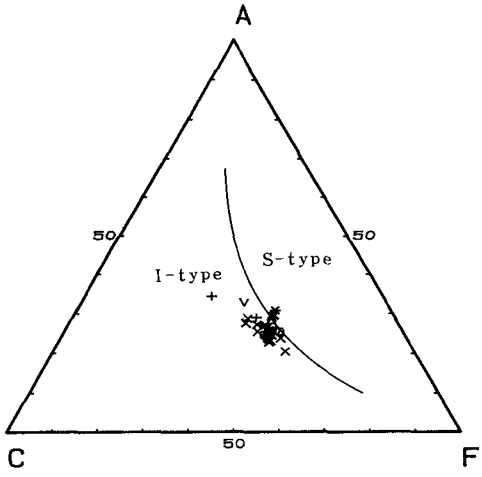

Fig. 39. Bulk composition of the volcano-plutonic rocks plotted in terms of (Al_2O_3 $-Na_2O-K_2O$) $-CaO-(FeO+MgO)$ in molecular %. (after White and Chappell, 1977) (Symbols are the same as in Fig. 18)

search Program. Special thanks should go to Dr. Choi, H.I. for his reviewing the manuscript. One of the writers(JMS) thanks Dr. Lee, J.S. and Mr. Shin, S.C., for their processing the data by computer and drawing the figures.

References

Adie, R.J., ed., 1962. Antarctic Geology. Amsterdam : North-Holland Publ. ; New York : Wiley Inter-Science, 758p.

Barton, C.M. 1965. The Geology of the South Shetland Islands : Ⅲ. The sratigraphy of King George Island. British Antarctic Survey Scientific Reports, No.44, 33p.

Davies, R.E.S. 1982. The Geology of the Marian Cove area, King George Island, and a Tertiary age for its supposed Jurassic volcanic rocks. British Antarctic Survey Scientific Reports, No.51, 151-165.

Evensen, N.M., P.J. Hamilton and R.K O'Nions. 1978. Rare-earths Abundances in chondritic meteorites. Geochim. Cosmochim Acta. 42 : 1199-1212.

Ferguson, D. 1921. Geological observations in the South Shetlands. The Palmer Archipelago and Graham Land, Antarctica. Trans. R. Soc. Edinb. 53, Pt. 1, No. 3, 29-55.

Grikurov, G.E., M.M. Krylov and Ya. N. Tsovbun. 1970. Age of rocks of the northern part of the Antarctic peninsula and the South Shetland Islands. Inf. Bull. Sov. Antarkt. Eksped. No. 80, 30-34.

Hawkes, D.D. 1961. The Geology of the South Shetland Islands : I. The Petrology of King George Island, Antarctica. Falkland Island dependenceis Survey Scientific Reports, No. 26, 28p.

Hong, G.H. 1989. Oceanography of Maxwell Bay, The King George Island : Short-Term Variation of Chemical Property of Water and Sedimentation of Particulate Matter in the Glacially-fed Antarctic Coastl Warters. In : H.T. Huh, B.K. Park, and S.H. Lee(eds), Antarctic Science : Geology and Biology. Kor. Ocean Res. Develop. Inst. 171-186.

Jin, M.S., M.S. Lee and P.C. Kang. 1989. Geology and Petrology around the Barton and Weaver Peninsula, King George Island, Antarctica. In : A Study on Natural Environment in ghe area around the Korean Antarctic station, King George Island(Ⅱ). BSPG 00081-246-7, 73-106.

Kang, P.C., and M.S. Jin. 1989. Petrology and Geologic Structures of the Barton Peninsula, King George Island, Antarctica. In : H.T. Huh, B.K. Park, S.H. Lee(eds.), Antarctic Science : Geology and Biology. Kor. Ocean Res. Develop. Inst. 121-135.

Lambert, R.St.J. and, J.G. Holland. 1974. Yttrium geochemistry applied to petrogenesis utilizing calcium-yttrium relationships in minerals and rocks. Geochim. Cosmochim. Acta, 38 : 1393-1414.

Meijer, A. 1982. Mariana-Volcano Islands.

In : R.S. Thorpe(ed.), Andesites, John Wiley and Sons. pp.293－306.

Miyashiro, A. 1974. Volcanic rock series in island arcs and active continental margins. Am. J. Sci., 274 : 321－355.

Miyashiro, A. 1978. Nature of alkalic volcanic rock series. Contri. Mineral Petrol., 66, 91－104

Park, B.K. 1989. Potassium-Argon Radiometric Ages of Volcanic and Plutonic Rocks from the Barton Peninsula, King George Island, Antarctica. Jour. Geol. Soc. Korea, 25 : 495－497.

Pearce, J.A., and J.R. Cann. 1973. Tectonic setting of basic volcanic rocks determined using trace element analyses. Earth Planet. Sci. Lett., 19 : 290－300.

Rex, D.C. 1976. Geochronology in relation to the stratigraphy of the Antarctic Peninsula. British Antarc. Surv. Bull., 43, 49－58.

Shoji, T and H. Kaneda, 1980. Classification of Igneous Rocks, Based on the Relationships among Nicke., Cobalt and Silica content. Mining Geol., 30, 289－298.

Smellie, J.L., R.J. Pankhurst, M.R.A. Thomson and R.E.S. Davies. 1984.
The Geology of the Shetland Islands, IV. Stratigraphy, Geochemstry and evolution. British Antarc. Surv. Bull., No. 87, 1－85.

Tarney, J.S.D., A.D. Weaver, R.J. Pankhurst, and P.F. Barker. 1982. Volcanic evolution of the northern Antarctic Peninsula and the Scotia arc. In : R.S.Thorpe(ed.), "Andesites" John Wiley & Sons, pp.371－400.

Thomson, M.R.A. 1972. New discoveries of fossils in the Upper Jurassic Volcanic group of Adelaide Island. British Antarc. Surv. Bull., No. 30, 95－101

Watt, D. R. 1982. Potassium-argon ages and paleomagnetic results from King George Island, South Shetland Islands. In : C. Craddock(ed.) Antarctic Geoscience, Madson, University of Wisconsin Press, 255－261.

White, A.J.R., and B.W. Chappell. 1977. Ultrametamorphism and granitoid genesis. Tectonophysics, 43 : 7－22.